Journal of Colloid and Interface Science 356 (2011) 325–330

Contents lists available at ScienceDirect

Journal of Colloid and Interface Science

www.elsevier.com/locate/jcis

Electrokinetics of charged spherical colloidal particles taking into account the effect of ion size constraints

J.J. López-García [a], M.J. Aranda-Rascón [a], C. Grosse [b,c], J. Horno [a,*]

[a] Departamento de Física, Universidad de Jaén, Campus Las Lagunillas, Ed. A-3, 23071 Jaén, Spain
[b] Departamento de Física, Universidad Nacional de Tucumán, Av. Independencia 1800, 4000 San Miguel de Tucumán, Argentina
[c] Consejo Nacional de Investigaciones Científicas y Técnicas, Avenida Rivadavia 1917, 1033 Buenos Aires, Argentina

ARTICLE INFO

Article history:
Received 3 November 2010
Accepted 16 December 2010
Available online 22 December 2010

Keywords:
Colloids
Electrokinetic phenomena
Finite ion size
Charge reversal

ABSTRACT

The electrokinetic properties of suspended spherical particles are examined using a modified standard electrokinetic model, which takes into account the finite ion size and considers that the minimum approach distance of ions to the particle surface need not be equal to their effective radius in the bulk solution. We calculate the conductivity increment and the electrophoretic mobility and present a detailed interpretation of the obtained results, based on the analysis of the equilibrium and field-induced ion concentrations, as well as the convective fluid flow in the neighborhood of the particle surface. We show that when charge reversal takes place, the sign of the concentration polarization remains unchanged while the sign of the electrophoretic mobility only changes under favorable circumstances.

1. Introduction

The classical description of electrokinetic phenomena in colloidal suspensions is based on a series of assumptions that constitute the standard electrokinetic model: suspended particles are surrounded by a uniform surface density of fixed charge; ions can be treated as mathematical points; macroscopic permittivity and viscosity values remain valid at the microscopic scale up to the very surface of the particle [1–5]. Despite its almost universal use, this model leads to inconsistencies such as unrealistically high counterion concentration values near highly charged particles, and fails to describe some experimental evidence such as the movement of colloidal particles in the opposite direction to that predicted by the sign of their charge [5].

In a recent work [6] we analyzed the effect of the finite ion size on the structure of the equilibrium double layer surrounding suspended particles. We considered that while different ion species have the same effective size in the bulk solution, their minimum approach distances to the particle surface have different values for each species. We showed that this last assumption leads to important quantitative changes to the structure of the equilibrium diffuse double layer. Furthermore, under favorable circumstances, a qualitative change should occur: the charge reversal phenomenon.

Although there are many previous works dealing with the finite ion size in colloidal suspensions [7–14], they are generally limited to the equilibrium properties of the system. On the contrary, the aim of the present work is to account for the effect of the ion size constraints on the dynamics of the system. We so examine the behavior of the considered model under the action of an applied DC electric field. We calculate the conductivity increment and the electrophoretic mobility, and present a detailed interpretation of the obtained results based on the analysis of the equilibrium and field-induced ion concentration and fluid flow profiles in the neighborhood of the particle.

We show that purely "physical" mechanisms can lead to the reversal of the electrophoretic mobility, even without taking into account electrostatic ion–ion or induced particle–ion correlations. Moreover, the conditions required for this phenomenon to occur are different from those needed to obtain charge reversal. It is possible, therefore, to have charge inversion without changing the sign of the electrophoretic mobility.

2. Theory

We consider a spherical particle of radius a immersed in an infinite electrolyte solution with m ionic species. The equations governing the steady-state dynamics of this system are well known:

(a) Nernst–Planck equations for the ionic flows,
(b) continuity equations for each ionic species,
(c) Poisson equation for the electric potential,
(d) Navier–Stokes equation for a viscous fluid, and
(e) continuity equation for an incompressible fluid.

* Corresponding author.
E-mail address: jhorno@ujaen.es (J. Horno).

0021-9797/$ - see front matter © 2010 Elsevier Inc. All rights reserved.
doi:10.1016/j.jcis.2010.12.063

For an ideal electrolyte solution, this set of equations together with the appropriate boundary conditions constitutes the standard electrokinetic model.

In order to treat nonideal solutions taking into account finite ion size, the activity coefficient γ_i ($\gamma_i = 1$ for an ideal solution) can be included in the diffusive term of the Nernst–Planck equations for the ion flows [15,16]:

$$c_i(\vec{r})\vec{v}_i(\vec{r}) = -D_i c_i(\vec{r})\nabla\left\{\ln\left[\gamma_i(\vec{r})c_i(\vec{r})\right] + \frac{z_i.e}{kT}\phi(\vec{r})\right\} + c_i(\vec{r})\vec{v}(\vec{r}). \quad (1)$$

Here $\vec{v}_i$, c_i, z_i, and D_i are the velocity, the local concentration (in mol/m^3), the signed valence, and the diffusion coefficient of the ionic species i (with $i = 1, \ldots, m$). The electric potential is represented by means of the symbol ϕ, $\vec{v}$ is the fluid velocity, e the elementary charge, k the Boltzmann constant, and N_A the Avogadro number.

As in our earlier works on this subject [6,15,17,18], we shall use for the activity coefficient an expression that is equivalent to the Bikerman formula [19],

$$\gamma_i = \gamma = \frac{1}{1 - \sum_{i=1}^{m} \frac{c_i}{c_i^{\max}}}, \quad (2)$$

where $c_i^{\max}$ are the highest possible concentration values for species i ions. These values are related to the effective ion radii R_i and to the considered ion packing

$$N_A c_i^{\max} = p\frac{3}{4\pi R_i^3}, \quad (3)$$

where the packing coefficient is $p = 1$ for perfect packing, $p = \pi/3\sqrt{2} \approx 0.74$ for close packing, $p \approx 0.64$ for random close packing [3], and $p = \pi/6 \approx 0.52$ for simple cubic packing. Combined with the equilibrium form of Eq. (1), the activity coefficient expression (2) leads to the following dependence of the ion concentrations on the dimensionless electric potential $y = e\phi/kT$:

$$c_i = \frac{c_i^{\infty} e^{-z_i y}}{1 + \sum_{i=1}^{m} \frac{c_i^{\infty}}{c_i^{\max}}(e^{-z_i y} - 1)}. \quad (4)$$

On the other hand, due to the finite ionic size and to the ion–particle surface interactions, we assume that ions of species i cannot come closer to the particle surface than an effective distance of minimum approach h_i, which need not be equal to their effective radius R_i. We consider as in [6] that these distances are ordered in such a way that $h_j \leqslant h_{j+1}$ for $j = (1, 2, \ldots m-1)$. Therefore, the region next to the particle surface can be divided into a series of layers such that for $a \leqslant r < a + h_1$ no ion centers are present, for $a + h_j \leqslant r < a + h_{j+1}$ only ionic species with $i \leqslant j$ are allowed, and for $a + h_m \leqslant r$ all ionic species are allowed.

The equations governing the steady-state dynamics of the system are first solved in equilibrium and then under the action of a weak DC electric field E_a. The perturbed equations are then linearized with respect to the applied field, referring the perturbed variables to their equilibrium values (upper index 0) plus a perturbation term (preceded by the character δ) and keeping in the final equations only the terms that are linear in the perturbations.

While the equilibrium equations and boundary conditions can be found in [6], a detailed account of the linearized equations together with the corresponding boundary conditions is given in Ref. [20] that deals with the DC behavior of soft particles (uncharged insulating particles surrounded by a polymer layer bearing a fixed charge density ρ^v through which ions can freely move while the fluid flow hindrance is characterized by a parameter λ):

- Inside the core of the particle the electric field is uniform.
- At the surface of the core the electric potential and the normal component of the displacement vector are continuous. The fluid velocity and the radial component of the ion velocities vanish.
- At the polymer layer–electrolyte solution interface, the electric potential, the normal component of the displacement vector, the fluid velocity, the chemical potentials of ions ($\mu_i = \ln(\gamma c_i)$), the ionic velocities, the vorticity ($\vec{\Omega} = \nabla \times \vec{v}$), and the pressure are continuous.
- Far from the particle, the electric potential reduces to that of the applied field and the fluid velocity to minus the electrophoretic velocity, while the field-induced perturbations of the ionic concentrations and the vorticity vanish.
- The total force acting on the particle vanishes.

From an analytical standpoint, the systems considered in the present work and in Ref. [20] only differ in the following aspects:

- There is no polymer inside the layer surrounding the particle so that the fixed charge density vanishes ($\rho^v = 0$) while the fluid flow is unhindered ($\lambda = 0$),
- the particle now bears a fixed surface charge,
- even in the simplest case of only two ion types ($m = 2$), the system includes an additional boundary: at $r = a + h_1$ and $r = a + h_2$,
- the Nernst–Planck equations include the activity coefficients, Eqs. (1) and (2).

The boundary conditions remain unchanged with one notable exception: the continuity of the chemical potentials at $r = a + h_j$ leads, in view of Eq. (4), to the discontinuity of the ion concentrations. This modifies the expressions used to determine the first derivative of the vorticity:

- At $r = a + h_j$: now obtained from the tangential component of the Navier–Stokes equation evaluated at $r = a + h_j^{\pm}$ and taking into account the continuity of the pressure:

$$\frac{\eta}{a+h_j}\frac{d}{dr}(r\Omega)\bigg|_{a+h_j^-} - \frac{\eta}{a+h_j}\frac{d}{dr}(r\Omega)\bigg|_{a+h_j^+} = eN_A\left[\sum_{i=1}^{m} z_i c_i^0(a+h_j^+) - \sum_{i=1}^{m} z_i c_i^0(a+h_j^-)\right]\frac{\delta\phi(a+h_j)}{a+h_j} \quad (5)$$

- At $r = a$: now obtained from the condition that the mechanical and electrical forces acting on the particle must be balanced and taking into account that the whole system is electroneutral:

$$eN_A\int_a^{\infty} r^2\frac{d\phi^0}{dr}\sum_{i=1}^{m} z_i c_i^0\left(\frac{\delta c_i}{c_i^0} + \frac{z_i e\delta\phi}{kT}\right)dr - eN_A a^2\sum_{i=1}^{m} z_i c_i^0(a^+)\delta\phi(a) + \eta a^3\frac{d\Omega}{dr}\bigg|_a - a^2\eta\Omega(a) + eN_A\sum_{j=1}^{m}\left\{(a+h_j)^2\delta\phi(a+h_j)\sum_{i=1}^{m} z_i\left[c_i^0(a+h_j^-) - c_i^0(a+h_j^+)\right]\right\} = 0 \quad (6)$$

where η is the fluid viscosity.

Note that neglecting the ionic size effects leads to the continuity of the ionic concentrations at $r = a + h_i$ and transforms Eqs. (5) and (6) into Eqs. (55) and (63) from [20].

These changes were unwillingly omitted in [17] where the conditions based on the original Eqs. (55) and (63) from [20] were used. Fortunately this had a very small incidence on the presented results because of the presence of a single boundary besides the particle surface. However, in the present case that includes at least two such boundaries, the use of the corrected boundary conditions is crucial.

The numerical calculations were performed using an algorithm based on the network simulation method, which consists in

modeling the governing differential equations by means of an electrical circuit. A full account of the network model used in this work is given in Ref. [20] and a more general explanation of the method is given in Ref. [21].

It must be noted that since the electric potential changes rapidly near the interface $r = a$, an appropriate simulation space grid must be modeled. In this work, the r-space grid is automatically adapted to the evolution of the electric potential profiles. If, in the course of the simulation, strong changes of y with r are detected in any r coordinate region, more grid points are added into that region. Appropriate simulation space grids were calculated in this way to ensure good accuracy and moderate CPU times.

3. Results and discussion

For sake of simplicity, all the simulations were performed considering just two ion types ($m = 2$), and using the parameter values shown in Table 1 (except when indicated otherwise).

We consider the particular case of a negative surface charge value because colloidal particles suspended in aqueous electrolyte solutions usually acquire a negative charge. Therefore counterions are positive (cations) while co-ions are negative (anions).

It was shown in the literature [22] that the typical value of the effective ionic solvated diameter, determined from mobility measurements, is approximately 0.6–0.8 nm. However, the effective ion size to be used in the considered theoretical model should be larger due to the ion–ion interactions [23]. The value of $c_i^{\max}$ for the two ionic species was chosen considering an effective solvated diameter in water of approximately 1 nm. On the other hand, the minimum approach distance to the particle surface has been chosen as $h_1 = 0.5$ for counterions while, for co-ions, the corresponding distance was left as a parameter $h_2 \geqslant h_1$.

The dependence on $h_2 - h_1$ of the equilibrium properties of the system has been extensively discussed in a previous paper [6]. The main qualitative conclusion is that because of the constraint on the co-ion presence in the $h_1 < r - a < h_2$ layer, the total electric charge of counterions in this layer can surpass the absolute value of the electric charge of the particle leading to charge reversal (see Fig. 2 in Ref. [6]). The condition for this phenomenon to occur, under the thin double layer approximation and for $c^{\max} \to \infty$, is [6]

$$h_2 - h_1 > \frac{1}{z_1 e}\sqrt{\frac{2kT\varepsilon_e}{c_1^{\infty} N_A}}\tan^{-1}\sqrt{\frac{\sigma_s^2}{2kT\varepsilon_e c_1^{\infty} N_A}}. \tag{7}$$

In what follows we show the behavior of the system under the action of a DC electric field $E_a = 1$ V/m. In view that the governing equations were linearized with respect to the applied field strength, this particular choice is equivalent to using any other value and dividing the results by E_a. Fig. 1 represents the field-induced counterion and co-ion concentration (δc_i) and charge density ($\delta\rho$) profiles and their dependence on the difference $h_2 - h_1$. For $h_2 - h_1 = 0$, the field-induced ion concentrations (Fig. 1a) have the expected behavior for a negative particle: the counterion profile starts with a maximum close to the particle while the co-ion starts with a minimum. The counterion concentration decreases with the distance to the particle while the co-ion concentration increases so that the two curves cross each other after which they converge to a common positive value at a distance of the order of the Debye screening length. At greater distances, of the order of the particle radius, this common value slowly decreases to zero, which corresponds to a positive field-induced increment of the electrolyte concentration, often referred to as "concentration polarization."

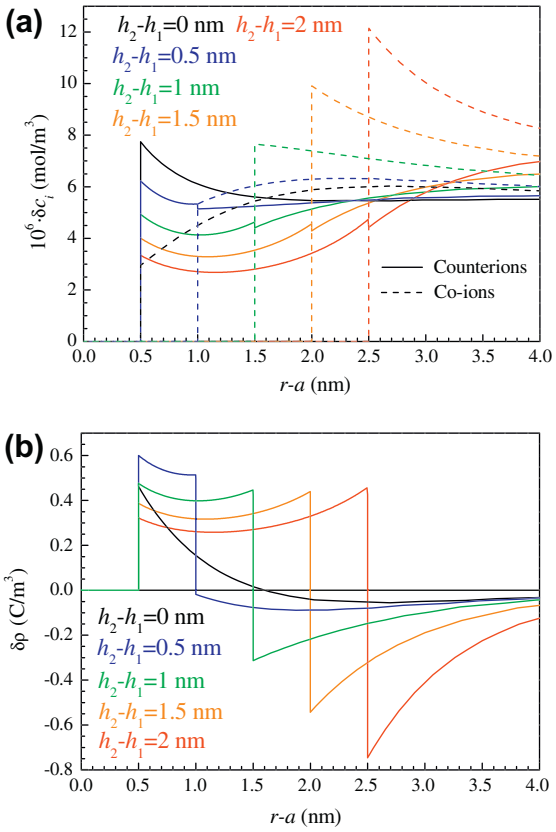

Fig. 1. Field-induced counterion and co-ion concentration and charge density profiles for $E_a = 1$ V/m, and their dependence on the difference $h_2 - h_1$. The remaining parameters are given in Table 1.

This characteristic behavior strongly changes with increasing $h_2 - h_1$ values: the field-induced counterion concentration close to the particle decreases while the corresponding co-ion concentration increases. At large $h_2 - h_1$ values (larger than those corresponding to charge reversal), counterions and co-ions exchange their roles so that anions have a higher field-induced concentration than cations. Note, however, that this concentration behavior does not fully correspond to that of a positive particle: outside the double layer the anion and cation concentrations still converge to a positive value. On the contrary, for a positively charged particle, the field-induced electrolyte concentration in the electroneutral region is negative.

This important qualitative difference is due to the nature of the equilibrium ion concentrations close to the particle: negative particles are normally surrounded by an excess layer of cations while positive particles attract anions. However, in the considered case of a negative particle and a $h_2 - h_1$ value sufficiently large as to produce charge reversal, the layer surrounding the particle is mostly formed by cations, not anions. Because of this layer, the steady-state field-induced cation and anion flows around the particle must be different: cations must converge toward the particle at a steeper angle (the cation surface conductivity larger than that of anions). This behavior requires field-induced ion concentration gradients at large distances that are similar to those corresponding to a

Table 1
Parameter values used in the calculations except when specified otherwise.

$\sigma_S = -0.02$ C/m^2	$a = 100$ nm	$z = z_1 = -z_2 = 1$
$c_1^{\infty} = 100$ mol/m^3	$h_1 = 0.5$ nm	$c_1^{\max} = 1500$ mol/m^3
$c_2^{\infty} = 100$ mol/m^3	$R_1 = R_2 = 0.5$ nm	$c_2^{\max} = 1500$ mol/m^3
$T = 298$ K	$\varepsilon_e = 78.54\varepsilon_0$	$\varepsilon_0 = 8.854 \times 10^{-12}$ F/m
$k = 1.381 \times 10^{-23}$ J/K	$N_A = 6.022 \times 10^{23}$ mol^{-1}	$e = 1.602 \times 10^{-19}$ C

negative particle: positive rather than negative values both for cations and anions.

Fig. 2 represents the conductivity increment ΔK defined by

$$K = K_e(1 + \varphi\Delta K) = K_e(1 + 3\varphi d)$$

as a function of the difference $h_2 - h_1$ and its dependence on the ion valence. In this expression K and K_e are the conductivities of the suspension and of the suspending medium, respectively, φ is the volume fraction occupied by the particles, and d the dipolar coefficient.

Fig. 2 shows unusually low conductivity increment values, even lower than those expected for uncharged insulating particles of radius a in a conducting medium such that $\kappa a \gg 1$ since, under these conditions, the dipolar coefficient would be $d = -1/2$ so that $\Delta K = -3/2$. The obvious reason is that in the considered model all ions types are excluded from the first layer of thickness h_1, which means that the equivalent insulating particle would have an effective radius $a + h_1$ rather than a. Therefore, the corresponding conductivity increment should have the value

$$\Delta K = 3\left(-\frac{1}{2}\right)\left(\frac{a+h_1}{a}\right)^3 = -\frac{3}{2}\left(\frac{105}{100}\right)^3 = -1.5226.$$

As can be seen, all the curves appearing in Fig. 2 have a higher value than this result, but only for $h_2 - h_1 = 0$. This is to be expected since, for $h_2 - h_1 > 0$, the effective radius of the particle becomes even larger: $a + h_2$ rather than $a + h_1$. The dashed line in Fig. 2 that corresponds to the equation

$$\Delta K = 3\left(-\frac{1}{2}\right)\left(\frac{a+h_2}{a}\right)^3 \tag{8}$$

lies lower than all the remaining curves. For any curve, the difference with respect to the dashed line is determined by the quotient of the surface conductivity of the particle and the conductivity of the suspending medium.

Fig. 3 represents the dimensionless tangential fluid velocity

$$\bar{v}_\theta = \frac{ae^2\eta}{(kT)^2\varepsilon_e} v_\theta$$

profiles and their dependence on the difference $h_2 - h_1$. In this expression v_θ are the fluid velocity values calculated at the particle equator: $\theta = \pi/2$. Note that in this figure the fluid velocity is referred to infinity, so that it tends to zero for $r - a \to \infty$. Therefore, the velocity at the particle surface is proportional to minus the electrophoretic velocity, v_e. Since in all the examined cases this value is positive, the resulting electrophoretic mobility is negative and does not change its sign when charge reversal occurs. As can be seen,

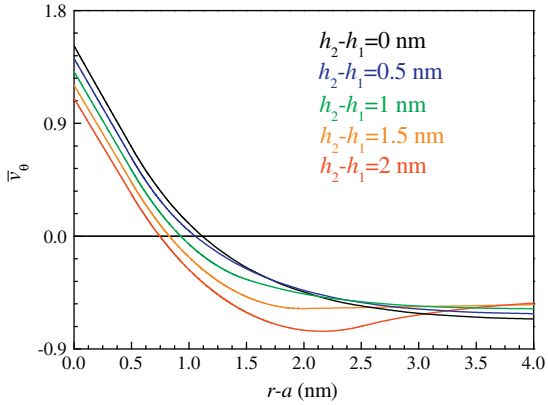

Fig. 3. Dimensionless tangential fluid velocity profiles (calculated at the particle equator: $\theta = \pi/2$), and their dependence on the difference $h_2 - h_1$. The remaining parameters are given in Table 1.

charge reversal only leads to the appearance of a pronounced minimum in the velocity profiles close to the particle surface. This behavior occurs because of the change of the equilibrium charge density sign for $r - a > h_2$ and sufficiently large $h_2 - h_1$ values for charge reversal to occur (see Fig. 2b in Ref. [6]).

Fig. 4 represents the dimensionless electrophoretic mobility

$$u_e = \frac{3e\eta}{2\varepsilon kT}\frac{v_e}{E_a}$$

as a function of the difference $h_2 - h_1$ and its dependence on the ion valence.

As can be seen, and in agreement with the preceding comments, the mobility values are always negative, as is usual for a negatively charged particle. As expected, the mobility decreases in absolute value with increasing ion valence since the surface potential decreases (see Fig. 4a in Ref. [6]). It also decreases with the difference $h_2 - h_1$, but does not reduce to zero and change sign when charge reversal takes place. While this result suggests that electrophoretic measurements would never reveal the kind of charge reversal described by the present model, this is actually not the case as will be shown in the following figure.

Fig. 5a and b represents the electrophoretic mobility and the conductivity increment as functions of the particle charge and their dependence on the difference $h_2 - h_1$. It should be noted that in these figures lower index 1 (2) corresponds to anions (cations) rather than to counterions (co-ions), as is the case in the rest of this

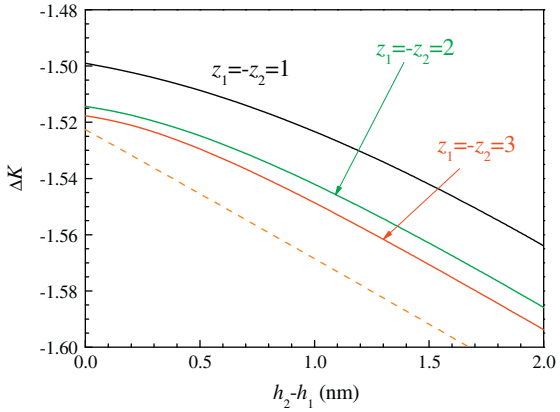

Fig. 2. Conductivity increment as a function of the difference $h_2 - h_1$ and its dependence on the ion valence. The remaining parameters are given in Table 1. The dashed line corresponds to the analytical solution, Eq. (8).

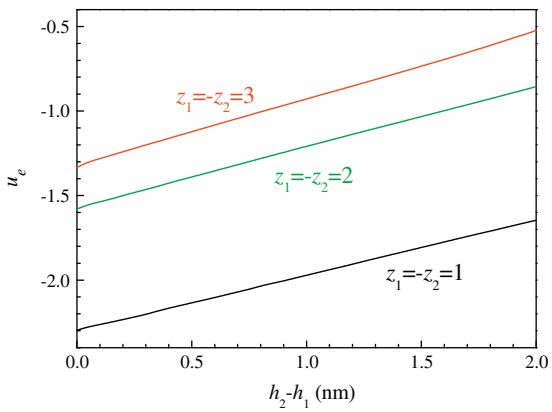

Fig. 4. Dimensionless electrophoretic mobility as a function of the difference $h_2 - h_1$ and its dependence on the ion valence. The remaining parameters are given in Table 1.

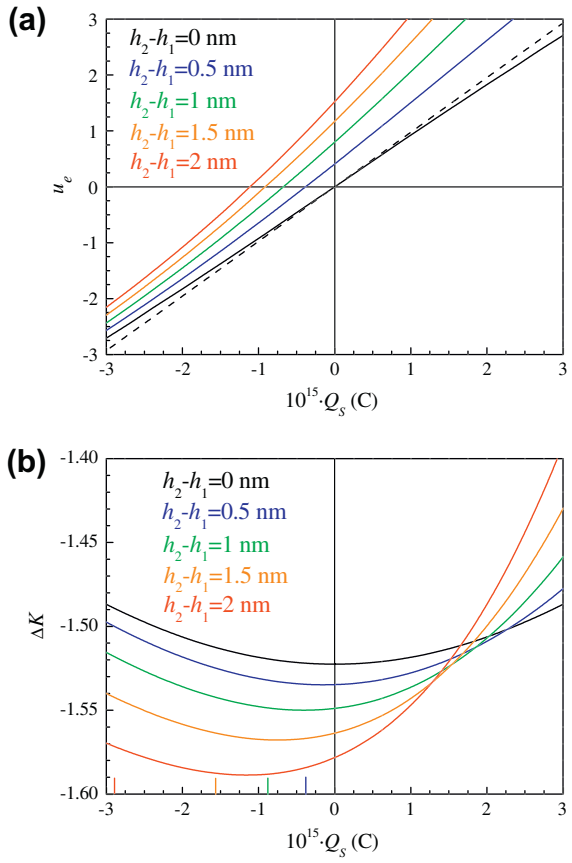

Fig. 5. Dimensionless electrophoretic mobility (a) and conductivity increment (b) as functions of the particle charge and their dependence on the difference $h_2 - h_1$. The remaining parameters are given in Table 1. The vertical segments represent the charge values calculated using Eq. (7); see text.

work. Therefore, when the particle charge changes from negative to positive, the first layer becomes populated only by co-ions rather than counterions. As expected, the mobility and conductivity increment curves corresponding to $h_2 - h_1 = 0$ are symmetrical with respect to the sign of the particle charge. On the contrary, this symmetry is lost for all the other $h_2 - h_1$ values.

The dashed line in Fig. 5a corresponds to the analytical solution for the electrophoretic mobility that is only valid for $h_2 - h_1 = 0$ and weakly charged particles. Under these conditions, Eqs. (4) and (7)–(10) in [6] lead to the following expression for the equilibrium dimensionless surface potential

$$y_0 = \frac{e\sigma_s}{kT\varepsilon_e}\left(\frac{1}{\kappa} + h_2\right)$$

which, combined with the Smoluchowsky expression

$$u_e = \frac{3}{2}y_0$$

gives

$$u_e = \frac{3e}{2kT\varepsilon_e}\frac{Q_s}{4\pi a^2}\left(\frac{1}{\kappa} + h_2\right).$$

Fig. 5a shows that for $h_2 - h_1 > 0$, the electrophoretic mobility can become positive even for negative values of the particle charge. However, this only occurs for sufficiently low (in modulus) values of the particle charge. This is why in Fig. 4, which corresponds to the surface charge value given in Table 1 ($Q_s \approx -2.5 \times 10^{-15}$ C), the electrophoretic mobility sign does not change for the considered $h_2 - h_1$ values.

Fig. 5b shows that the conductivity increment corresponding to $h_2 - h_1 = 0$ attains a minimum for uncharged particles and increases with the particle charge as the surface conductivity increases. At the minimum, the conductivity increment coincides with the expected value $\Delta K \approx -1.5226$ while, for increasing values of the difference $h_2 - h_1$, the conductivity increment decreases in view of the increase of the effective particle size (see comment of Fig. 2).

A less evident feature shown in Fig. 5b is the shift to negative particle charge values of the minima of the different curves with increasing $h_2 - h_1$ values. The origin of this behavior is that for $h_2 - h_1 > 0$, the equilibrium potential of an uncharged particle is positive, as can be seen in Fig. 5 in [6]. Therefore, under these conditions, the surface conductivity does not attain its minimum value since it is due both to the counterions in the $a + h_1 < r < a + h_2$ layer and to the two ion types in the diffuse double layer $r > a + h_2$. Decreasing the particle charge decreases the potential at $r = a + h_2$ so that the surface conductivity of the diffuse layer decreases while the conductivity of the counterion layer increases as it gets more populated. The conductivity increment minimum is attained somewhere close to the condition that the surface conductivity of the diffuse double layer vanishes, which corresponds to the charge reversal condition, Eq. (7). The particle charge values corresponding to this condition are represented by vertical segments in Fig. 5b. For even lower particle charge values both the counterion layer and the diffuse layer conductivities increase so that the conductivity increment also increases.

Fig. 6a and b represents the electrophoretic mobility and the conductivity increment as functions of the electrolyte concentration and their dependence on the difference $h_2 - h_1$. As can be seen, these magnitudes only depend on this difference for high electrolyte concentrations so that the default value of 100 mol/m^3 used in this work, Table 1, lies right in the middle of the range where this dependence occurs.

The $h_2 - h_1 = 0$ mobility curve shows the well-known behavior [24]: Debye–Hückel limit at low electrolyte concentrations and Smoluchowsky value for the opposite limit. For high electrolyte concentrations, the mobility decreases (in modulus) with the difference $h_2 - h_1$ in agreement with Fig. 4, then vanishes, and finally becomes positive, just as in Fig. 5a. The huge increase of the mobility with the difference $h_2 - h_1$ at very high electrolyte concentrations is due to the corresponding increase of the surface potential. Under normal conditions and keeping constant the charge of the particle, the modulus of the surface potential always decreases with increasing electrolyte concentration, due to the decrease of the Debye screening length. However, in the considered case and with $h_2 - h_1 > 0$, an increase of the electrolyte concentration necessarily leads to charge reversal and, from there on, to an increase of the surface potential caused by the increasing number of cations in the counterion layer (see Fig. 3 in Ref. [6]).

The $h_2 - h_1 = 0$ conductivity increment curve shows the expected dependence on the electrolyte concentration at a fixed particle charge. At low concentrations the conductivity increment increases, because the surface conductivity remains essentially constant while the electrolyte solution conductivity decreases. This increases the dipole coefficient value that tends to the theoretical maximum $d = 1/4$ (valid under the thin double layer approximation). However, in the considered case of a relatively low surface charge, Table 1, a large surface potential is only attained at very low concentrations for which the thin double layer approximation breaks down. Correspondingly, the dipole coefficient should surpass the above-noted value in view of the larger size of the effective particle that includes its thick double layer (this expected limiting behavior lies outside the boundaries of Fig. 6b).

For increasing concentrations the electrolyte solution conductivity increases so that the conductivity increment decreases

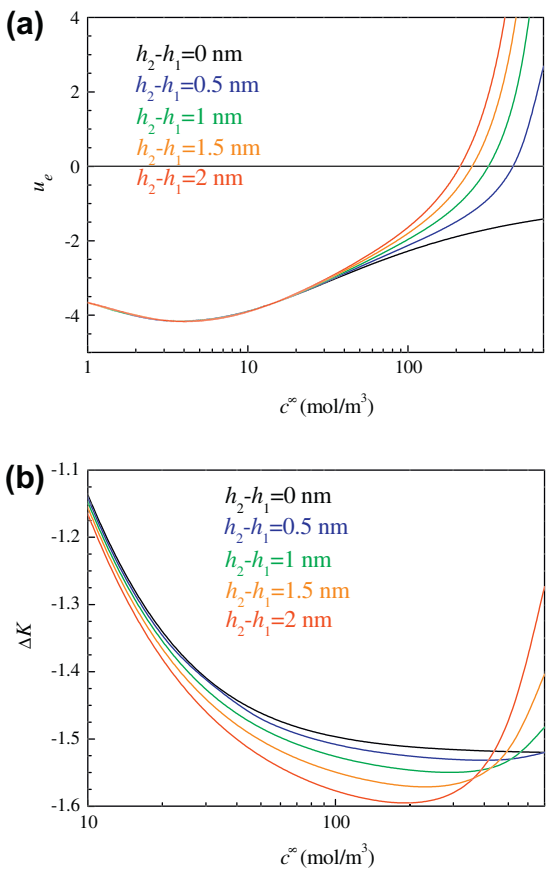

Fig. 6. Dimensionless electrophoretic mobility (a) and conductivity increment (b) as functions of the electrolyte concentration and their dependence on the difference $h_2 - h_1$. The remaining parameters are given in Table 1.

together with the surface potential and the double layer thickness, tending to a limiting value close to $-3/2$, as already discussed. Finally, when the double layer thickness decreases down to values that are comparable to the difference $h_2 - h_1$, the conductivity increment becomes a function of this parameter. As discussed in Fig. 2b, ΔK decreases with increasing $h_2 - h_1$ as the equivalent particle becomes larger. However, this qualitative behavior drastically changes at very high concentrations when the conductivity increment starts to increase with the difference $h_2 - h_1$. As noted above, this occurs after charge reversal takes place so that the cation density in the counterion layer rapidly grows, leading to a fast increase of the surface conductivity.

4. Conclusion

We present an extension into the steady-state domain of a previous work that modifies the standard electrokinetic model by taking into account the finite ion size and considering that the minimum approach distance of ions to the particle surface need not be equal to their effective radius in the bulk solution. For sake of simplicity, our calculations correspond to the case of just two ion species, equal counterion and co-ion effective size in the bulk solution, and a larger minimum approach distance to the particle surface for co-ions than for counterions.

We examine the response of this model under the action of an applied DC electric field and calculate the conductivity increment and the electrophoretic mobility. We show that the sign of the concentration polarization, as determined by the sign of the particle charge, remains unchanged, even when charge reversal takes place. Furthermore, under these same conditions, the sign of the electrophoretic mobility does not change either, except for specially favorable circumstances: very low particle charge or high electrolyte concentration.

Our main qualitative conclusion is that purely "physical" mechanisms (difference between minimum approach distances) suffice to produce both charge reversal and change of the sign of the electrophoretic mobility. However, observation of this second phenomenon is not a good indication of the occurrence of the first since charge reversal may well occur without a change of the electrophoretic mobility sign.

Acknowledgments

Financial support for this work by Ministerio de Ciencia e Innovación (project FIS2010-19493), FEDER funds, and Junta de Andalucía (project PE-2008 FQM-3993) of Spain and by CIUNT (project 26/E419) of Argentina is gratefully acknowledged.

References

[1] J.Th.G. Overbeek, Koll. Beihefte 54 (1942) 287.
[2] R.W. O'Brien, L.R. White, J. Chem. Soc., Faraday Trans. 2 (74) (1978) 1607.
[3] W.B. Russel, D.A. Saville, W.R. Schowalter, Colloidal Dispersions, Cambridge Univ. Press, 1995.
[4] R.J. Hunter, Foundations of Colloid Science, vol. I, Oxford Univ. Press, London, 1995.
[5] J. Lyklema, Fundamentals of Colloid and Interface Science, vol. II, Solid/Liquid Interfaces, Academic Press, London, 1995.
[6] J.J. López-García, M.J. Aranda-Rascón, C. Grosse, J. Horno, J. Phys. Chem. B 114 (2010) 7548.
[7] T. Das, D. Bratko, L.B. Bhuiyan, C.W. Outhwaite, J. Phys. Chem. B 99 (1995) 410.
[8] S. Woelki, H.H. Kohler, Chem. Phys. 261 (2000) 411.
[9] K. Bohinc, V. Kralj-Iglic, A. Iglic, Electrochim. Acta 46 (2001) 3033.
[10] F. Jimenez-Angeles, M. Lozada-Cassou, J. Phys. Chem. B 108 (2004) 7286.
[11] J.J. López-García, M.J. Aranda-Rascón, J. Horno, J. Colloid Interface Sci. 316 (2007) 196.
[12] A. Diehl, Y. Levin, J. Chem. Phys. 129 (2008) 124506.
[13] J.G. Ibarra-Armenta, A. Martín-Molina, M. Quesada-Pérez, Phys. Chem. Chem. Phys. 11 (2009) 309.
[14] L.B. Bhuiyan, C.W. Outhwaite, J. Colloid Interface Sci. 331 (2009) 543.
[15] J.J. López-García, M.J. Aranda-Rascón, J. Horno, J. Colloid Interface Sci. 323 (2008) 146.
[16] P. Strating, F.W. Wiegel, Physica A 193 (1993) 413.
[17] M.J. Aranda-Rascón, C. Grosse, J.J. López-García, J. Horno, J. Colloid Interface Sci. 335 (2009) 250.
[18] M.J. Aranda-Rascón, C. Grosse, J.J. López-García, J. Horno, J. Colloid Interface Sci. 336 (2009) 857.
[19] J.J. Bikerman, Philos. Mag. 33 (1942) 384.
[20] J.J. López-García, C. Grosse, J. Horno, J. Colloid Interface Sci. 265 (2003) 327.
[21] J.J. López-García, J. Horno, in: J. Horno (Ed.), Network Simulation Method, Research Signpost, Trivandrum, 2002, p. 107.
[22] E.R. Nightingale, J. Phys. Chem. 63 (1959) 1381.
[23] M.Z. Bazant, M.S. Kilic, B.D. Storey, A. Ajdari, Adv. Colloid Interface Sci. 152 (2009) 48.
[24] P.H. Wiersema, A.L. Loeb, J.Th.G. Overbeek, J. Colloid Interface Sci. 22 (1966) 78.